

**ERROR ANALYSIS OF COMBINED  
OPTICAL-FLOW AND STEREO  
PASSIVE RANGING**

Yair Barniv

NASA/Ames Research Center

Moffett Field CA

July 2, 1997

# Contents

<b>1</b>	<b>Introduction</b>	<b>4</b>
<b>2</b>	<b>Passive Ranging</b>	<b>6</b>
2.1	Stereo Method . . . . .	7
2.2	Monocular Optical Flow Method . . . . .	8
<b>3</b>	<b>Cramer-Rao Lower Bound for OF Passive Ranging</b>	<b>8</b>
3.1	The Cramer-Rao Lower Bound (CRLB) . . . . .	9
3.2	Evaluating the terms in the CRLB for monocular OF . . . . .	11
<b>4</b>	<b>The CRLB for combined Optical Flow and Stereo</b>	<b>12</b>
4.1	Extension of the general derivation . . . . .	12
4.2	Interpretation of the Results . . . . .	14
4.2.1	Least Squares Achieves the CRLB . . . . .	14
4.2.2	Error Ellipses Never Intersect . . . . .	15
4.3	Evaluating the CRLB for stereo/OF . . . . .	17
4.4	Small-angle approximations to the CRLB for stereo/OF . . . . .	18
<b>5</b>	<b>Simulation Results</b>	<b>19</b>
<b>6</b>	<b>Summary and Conclusions</b>	<b>28</b>

## List of Figures

1	The stereo geometry . . . . .	6
2	The Optical-Flow geometry for two consecutive frames . . . . .	7
3	General sensor—object geometry . . . . .	10
4	The traveling-stereo geometry . . . . .	12
5	Error ellipses: $b_s = 0$ (t), $= 1$ m (b), $V = 15$ m/s, no misalignment. . . .	20
6	Error ellipses: $b_s = 2$ (t) $= 4$ m (b), $V = 15$ m/s, no misalignment. . . .	20
7	Case similar to figure 5 but with $V = 10$ m/s . . . . .	21
8	Depth errors for $b_s = 0, 1, 2, 3, 4$ m, $V = 15$ m/s, no misalignment . . . .	22
9	Case similar to figure 8 but with $V = 10$ m/s . . . . .	23
10	Misalignment sensitivity factor for $V = 10$ m/s, $y = 10$ m to 50 m . . . .	23
11	Error ellipses for $V = 10$ m/s, $y=10$ to 50 m, $\sigma_\phi = 2^\circ$ , $\sigma = 0.1^\circ$ , $b_s = 0$ m . . . .	24
12	Similar to figure 11 but with $b_s = 1$ m . . . . .	25
13	Effect of stereo baseline, $V = 10$ m/s, $\sigma_\phi = 2^\circ$ , $\sigma = 0.1^\circ$ , $b_s=0$ to 2 m . . . .	26
14	Effect of misalignment, $b_s=0$ m, $V=10$ m/s, $y=25$ m $\sigma_\phi=0$ to $4^\circ$ , $\sigma=0.1^\circ$ . . . .	26
15	Same as figure 14 except that $b_s = 1$ m . . . . .	27

# ERROR ANALYSIS OF COMBINED OPTICAL-FLOW AND STEREO PASSIVE RANGING

Yair Barniv

NASA/Ames Research Center

Moffett Field, CA 94035

key words: Optical Flow, Passive Ranging, Stereo Ranging, Triangulation, Error Analysis.

## Abstract

The motion of an imaging sensor causes each imaged point of the scene to describe a time trajectory on the image plane. The trajectories of all imaged points are reminiscent of a flow (*e.g.*, of liquid) which is the source of the term “optical flow”. Optical-flow ranging is a method by which the stream of two-dimensional images obtained from a forward-looking forward-moving passive sensor is used to compute range to points in the field of view. Another well-known ranging method consists of triangulation based on stereo images obtained from at least two stationary sensors. In this paper we analyze the potential accuracies of a combined optical flow and stereo passive-ranging system in the context of helicopter nap-of-the-earth obstacle avoidance. The Cramer-Rao lower bound is developed for the combined system under the assumption of a random angular misalignment common to both cameras of a stereo pair. It is shown that the range accuracy degradations caused by misalignment is negligible for a combined optical-flow and stereo system as compared to a monocular optical-flow system.

## 1 Introduction

Helicopters flying covert nap-of-the-earth missions need a means for passive ranging in order to navigate around terrain obstacles. Two main passive-ranging methods can potentially be employed for this purpose; one based on motion and the resulting image-plane optical flow (OF), and the other based on stationary stereo. Both methods can be thought of as special cases of a more general location method known in the literature as “bearing-only ” or “direction-of-arrival” (DOA) location (or localization). The term “ranging” refers to determining range alone —implicitly assuming that the cross-range is known— whereas, by location, we mean determining *both* coordinates in the plane. In the sequel we use the noun “depth” rather than “range” for the sensor/object distance along the line of sight (LOS) but we still prefer “ranging” on “depthing”.

DOA algorithms date back to 1947 (The Stansfield Algorithm [1]) and have been used in many diverse areas such as submarine tracking through sonar measurements, locating transmitters and radar sources for Elint (Electronic Intelligence), and locating guns using acoustic sensors. This is why the wealth of literature in those other areas is directly applicable to the problem at hand.

In passive ranging by stereo, the cameras are normally placed on a line perpendicular to the aircraft longitudinal body axis and the objects of interest (obstacles) are located in a small angular sector in front of the vehicle. Locating the obstacles in the vehicle’s coordinate system can be done by straightforward triangulation using a single stereo-pair measurement. The effect of multiple ( $N$ ) stereo measurements from a stationary camera pair is simply to reduce the rms of the location errors by  $\sqrt{N}$ . The location accuracy improves proportionate to the stereo-baseline length.

Optical-flow based ranging uses images obtained from a single camera but at different times associated with different locations along the flight path. The baseline in this case is created by the vehicle’s motion. As a result, this baseline —although it can be made long— is oriented along the flight path which is the worst possible geometry for

triangulation of head-on objects. Determining the effect of multiple measurements (taken along the baseline) on the location accuracy is not trivial because the geometry of every pair of measurements is different.

The relationship between the stereo and OF location methods can be summarized as follows. Both methods use the geometrical principle of triangulation to solve for the obstacle's location. In stereo, the baseline (distance between cameras) is fixed like an aperture of a real antenna, whereas in OF, the baseline is synthetic because it is created only due to the motion. For readers familiar with radar antennas, OF can be likened to a Synthetic Aperture Radar (SAR) that almost looks forward. The SAR's angular accuracy, similar to the OF depth accuracy, degrades as observed objects approach the flight path or, in OF terminology, the Focus of Expansion (FOE). The depth-measurement error, as the angular accuracy of a SAR, is infinite in that direction.

The complementing properties of stereo and OF ranging led us to investigate the performance of a combined stereo/OFF ranging method in which each one of the stereo cameras provides its OF imagery resulting from a common forward motion. However, there is yet another strong incentive to go in that direction as explained next. Field implementation of the OF method involves an accurate alignment of the optical axis with that of the inertial navigation system (INS) axis as determined by its initialization. In practice, this alignment error can be of the order of  $2^0$  which, as shown later, would result in large ranging errors. Implementation of stereo requires the alignment of two cameras with the INS —resulting in misalignments, say,  $b_1$  and  $b_2$ . Each error by itself is of the same order of magnitude as for a single camera, however, the *relative* misalignment,  $|b_1 - b_2|$  can be made an order of magnitude smaller because it involves aligning two similar optical sensors as opposed to aligning an optical sensor with the INS; for this reason, the derivation in this paper assumes  $b_1 = b_2$ . We have found that a combined stereo/OFF system can reduce the sensitivity to misalignment of a monocular OF by an order of magnitude.

Most of the DOA literature revolves around algorithm development, such as in [1, 2,

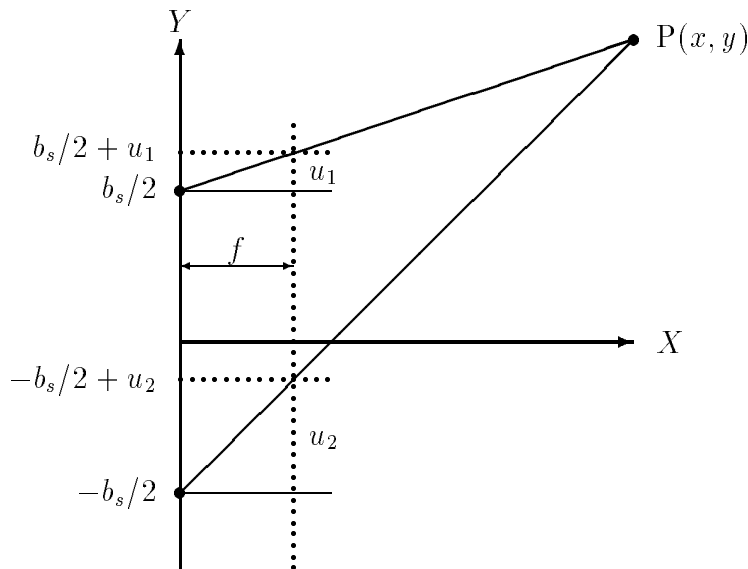


Figure 1: The stereo geometry

3], and accuracy estimation, such as in [4, 5, 6]. Similarly, passive ranging, mainly through OF, has concentrated on algorithm development [7, 8, 9, 10] and accuracy estimation [7, 11]. Accuracy estimation can be done on particular location algorithms or in terms of algorithm-independent bounds — which is where the present work belongs.

This paper starts (section 2) with the basic single-measurement accuracy of OF and stereo as given by Sridhar and Suorsa[11]. We then extend these results to the multiple-measurement case building upon the work of Wegner [5] and Gavish/Fogel [6] which is summarized in sections 3.1 and 3.2. The latter two works develop the Cramer-Rao Lower Bound (CRLB) for a single-sensor DOA problem without [5] and with [6] misalignment error. Our extension to the stereo case is developed in section 4. Simulation results and their interpretation are given in section 5.

## 2 Passive Ranging

In this section we discuss the simplest form of the two basic passive-ranging methods, motion or monocular OF, and stationary stereo, as they are used separately.

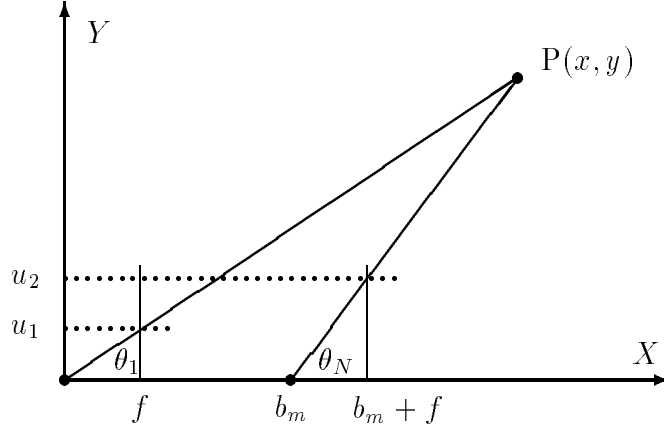


Figure 2: The Optical-Flow geometry for two consecutive frames

## 2.1 Stereo Method

Let us start with the stereo method because it is simpler to understand in terms of triangulation. The geometry of this case is shown in figure 1. The focal points of two cameras of equal focal length  $f$  are located at  $x = 0$ ,  $y = \pm b_s/2$ , and their optical axes are parallel to the  $X$ -axis. The focal planes are represented by the vertical dotted line at  $x = f$ . A point object at  $P(x, y)$  casts its images at  $y = -b_s/2 + u_2$  for the bottom camera and at  $y = b_s/2 + u_1$  for the top camera. From geometry of similar triangles,

$$u_1 = f(y - b_s/2)/x ; \quad u_2 = f(y + b_s/2)/x \quad (1)$$

which can be solved for the depth of the object,  $x$ :

$$x = fb_s/(u_2 - u_1); \quad (2)$$

Error analysis under the assumption  $x \gg b_s$  yields (see [11])

$$\sigma_x = \frac{\sqrt{2}x^2\sigma_u}{b_s f} \quad (3)$$

where  $\sigma_u$  is the rms of the error in determining  $u$ .

From (3) the depth estimate error is proportional to the square of the depth,  $x$ , it is independent of the lateral distance,  $y$ , and it is inversely proportional to the baseline distance  $b_s$ .

## 2.2 Monocular Optical Flow Method

Figure 2 shows the geometry for a degenerate OF which is based on two consecutive frames only. The (single) camera is similar to those of figure 1; its focal point is initially (at  $t = 0$ ) located at the origin of the coordinate system and its focal plane at  $x = f$ . An object at  $P(x, y)$  casts its image at  $y = u_1$ . When the camera moves (for the second frame) to a point  $x = b_m$ , the image of the same (stationary) object appears at  $y = u_2$ .

Typically, the distance  $b_m$  is small compared to the distance  $x$ , which implies that  $u_1 \approx u_2$ . This can thus be regarded as an equivalent stereo configuration having a baseline of  $b_m \sin \theta \approx b_m u_1 / f$ . Substituting that in (2) and (3) yields the depth and its accuracy as

$$x = b_m u_1 / (u_2 - u_1) ; \quad \sigma_x = \frac{\sqrt{2} x^2 \sigma_u}{b_m u_1} \quad (4)$$

It is now clear that the main difference between OF and stereo, as far as the depth accuracy is concerned, is in the definition of the baseline; the OF baseline is proportional to the inter-frame forward-motion,  $b_m$ , and to the angle,  $\theta$ , measured from the flight direction. This is why, in OF, depth accuracy degrades as the object gets closer to the FOE, *i.e.*,  $u_1$  in (4) decreases.

## 3 Cramer-Rao Lower Bound for OF Passive Ranging

So far, the basic accuracies of each ranging method were found separately. Two consecutive frames from a single camera have been used for OF and two concurrent frames from different cameras for stereo. Two relevant questions here are: (1) what accuracies can be obtained by each method separately in the case of multiple measurements, and (2) similarly for a combined method that uses the optical flows of two cameras in a stereo configuration (referred to as stereo/OF). In this section we develop expressions for the best achievable accuracies, based on the Cramer-Rao Lower Bound (CRLB) and special-

ize them to monocular OF-based passive ranging. In the next chapter the results are extended to the combined stereo/OFF system.

### 3.1 The Cramer-Rao Lower Bound (CRLB)

A standard problem in parameter estimation involves estimating a real non-random parameter vector,  $\beta$ , as  $\hat{\beta}(\theta)$ , given the observations,  $\theta$ , which depend on  $\beta$ . Many estimators are available of which some are unbiased. The Cramer-Rao inequality provides a lower bound on the covariance of the estimation error of *any* unbiased estimate of  $\beta$ . This bound defines the smallest attainable error ellipsoid in the parameter-vector space such that ellipsoids defined by any other unbiased estimator either lie outside or coincide with it; no intersection can occur. The error ellipse applicable to passive location in the plane is defined in the Appendix. In this section we use the CRLB in the form developed by Wegner [5] and Gavish/Fogel [6], and we thus follow their work for completeness. For further detail the reader is advised to consult these two works.

Let us assume that the measurement vector has a multivariate normal distribution with mean  $m$  (the measurement model) and covariance matrix  $\Sigma$ , that  $F(m, \beta) = 0$  is a given vector of constraints, and that  $F_m = \partial F / \partial m$  and  $F_\beta = \partial F / \partial \beta$  are continuous (which holds in our problem). The CRLB of an unbiased estimator of the parameter vector  $\beta$  is given by

$$S_\beta = [F_\beta^T (F_m \Sigma F_m^T)^{-1} F_\beta + J]^{-1} \quad (5)$$

where  $T$  denotes matrix transposition, and  $J$  is an information matrix reflecting any a priori knowledge about  $\beta$ .

Now consider the case shown in figure 3, where the sensor, generally located at  $x_i, y_i$ , measures the angles  $\theta_i$  to a stationary point  $P(x, y)$  with a misalignment of  $\phi$  (same  $\phi$  is added to all angular measurements although it is shown only once). Further, assume that the sensor is traveling along the  $X$ -axis<sup>1</sup> and produces angular measurements from points along its trajectory having  $x_i = b_m(i - 1)/(N - 1)$ , where  $N$  is total number of

---

<sup>1</sup>Although in this work we consider a straight trajectory as a tractable example, a similar derivation

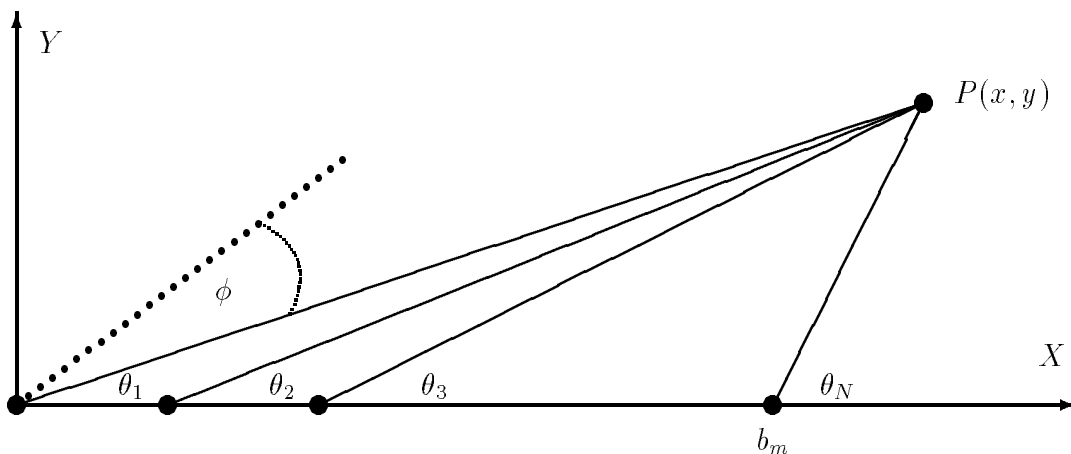


Figure 3: General sensor—object geometry

measurements. The angular measurements are

$$\theta_i = \tan^{-1}(\Delta y_i / \Delta x_i) + \phi + n_i, \quad i = 1, 2, \dots, N \quad (6)$$

where

$$\Delta y_i \triangleq y - y_i; \quad \Delta x_i \triangleq x - x_i \quad (7)$$

and  $n_i$  are independent noise samples out of a Normal distribution having variance  $\sigma^2$ .

The components of the measurement vector mean,  $m$ , are similar to the  $\theta_i$  of (6) in which the  $n_i$  terms are omitted. As a result,  $F_m$  equals the  $N \times N$  identity matrix  $I_N$ . Since the noise covariance matrix is diagonal,  $\Sigma = \sigma^2 I_N$ . Also, considering the misalignment as a random variable to be estimated, having a zero-mean normal distribution with variance  $\sigma_\phi^2$ ,  $J = \text{diag}(0, 0, \sigma_\phi^{-2})$ . No prior information is assumed about  $(x, y)$ . The vector to be estimated is  $\beta = (x, y, \phi)$ ; it is composed of the object location *and* the unknown misalignment.

Differentiating the constraint equations (6) with respect to the estimation vector  $\beta$  yields

$$F_\beta = [G \ 1_N] \quad (8)$$

---

could proceed with any other deterministic trajectory

where

$$G \triangleq \begin{bmatrix} -\Delta y_1/r_1^2 & -\Delta y_2/r_2^2 & \cdots & -\Delta y_N/r_N^2 \\ \Delta x_1/r_1^2 & \Delta x_2/r_2^2 & \cdots & \Delta x_N/r_N^2 \end{bmatrix}^T, \quad (9)$$

$r_i^2 \triangleq \Delta x_i^2 + \Delta y_i^2$ ;  $i = 1, 2, \dots, N$ , and  $1_N$  is a unity vector of length  $N$ . Substituting  $F_m$ ,  $F_\beta$ ,  $\Sigma$  and  $J$  into (5) yields

$$S_\beta = \left\{ [G \ 1_N]^T (\sigma^2 I_N)^{-1} [G \ 1_N] + \text{diag}(0, 0, \sigma_\phi^{-2}) \right\}^{-1} = \sigma^2 \begin{bmatrix} V^{-1} & H \\ H^T & (\sigma/\sigma_\phi)^2 + N \end{bmatrix}^{-1} \quad (10)$$

where  $H$  and  $V$  are defined as

$$H \triangleq G^T 1_N; \quad V \triangleq (G^T G)^{-1} \quad (11)$$

The CRLB  $S$  on the location estimation  $(x, y)$  is given by the  $2 \times 2$  upper-left corner of  $S_\beta$ , that is,

$$S = \sigma^2 \left[ V + \frac{V H H^T V}{(\sigma/\sigma_\phi)^2 + N - H^T V H} \right] \quad (12)$$

which is the result obtained by Gavish and Fogel in [6].

### 3.2 Evaluating the terms in the CRLB for monocular OF

The summations involved in  $H$  and  $V$  of (11) can be approximated by integrals (assuming  $N \gg 1$ ). When the sensor travels on the  $X$ -axis,  $y_i = 0$ , so that, in (7),  $\Delta y_i = y$ . Denoting the elements of the  $2 \times 2$  matrix  $G^T G$  of (11) by  $g_{ij}$ ,  $i, j = 1, 2$ , the element  $g_{11}$  can be found as

$$g_{11} = \sum_{i=1}^N \Delta y_i^2 / r_i^4 \approx \frac{N y^2}{b_m} \int_{x_1}^{x_N} \frac{1}{(y^2 + x^2)^2} dx \quad (13)$$

where  $b_m = x_N - x_1$ . Performing the integration and using the notation  $\theta_d \triangleq \theta_N - \theta_1$  and  $\theta_s \triangleq \theta_N + \theta_1$  with  $\theta_1$  and  $\theta_N$  defined in figure 3 to be the initial and last observation angles, yields

$$\begin{aligned} g_{11} &= \frac{N}{2b_m y} \left[ xy/(y^2 + x^2) + \tan^{-1}(x/y) \right]_{x_1}^{x_N} \\ &= \frac{N}{2b_m y} \left[ -\frac{1}{2} \sin 2\theta + \theta - \pi/2 \right]_{\theta_1}^{\theta_N} = \frac{N}{2b_m y} (-\sin \theta_d \cos \theta_s + \theta_d) \end{aligned} \quad (14)$$

The other three terms of  $G^T G$  and the two needed for  $H$  can similarly be found, so that (11) becomes

$$H \approx \frac{N}{b_m} \left[ -\theta_d \quad \ln \frac{\sin \theta_N}{\sin \theta_1} \right]^T; \quad G^T G = \frac{N}{2b_m y} \begin{bmatrix} \theta_d - \sin \theta_d \cos \theta_s & -\sin \theta_s \sin \theta_d \\ -\sin \theta_s \sin \theta_d & \theta_d + \sin \theta_d \cos \theta_s \end{bmatrix} \quad (15)$$

and

$$V = (G^T G)^{-1} = \frac{2b_m y}{N(\theta_d^2 - \sin^2 \theta_d)} \begin{bmatrix} \theta_d + \sin \theta_d \cos \theta_s & \sin \theta_s \sin \theta_d \\ \sin \theta_s \sin \theta_d & \theta_d - \sin \theta_d \cos \theta_s \end{bmatrix} \quad (16)$$

## 4 The CRLB for combined Optical Flow and Stereo

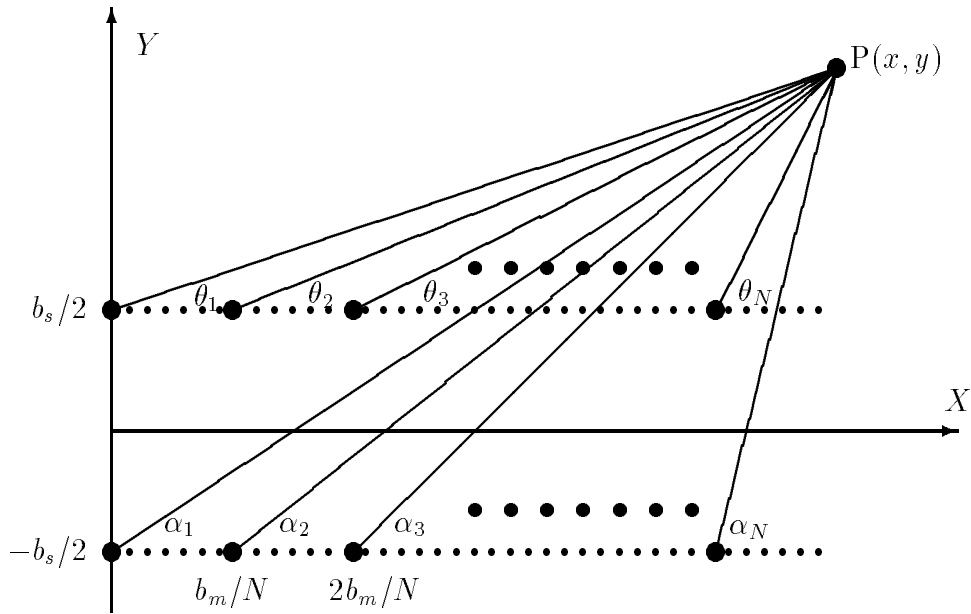


Figure 4: The traveling-stereo geometry

The above derivation is extended in this section to the case where optical flows from two cameras in a stereo configuration are observed in parallel.

### 4.1 Extension of the general derivation

The derivation of the CRLB for a pair of traveling cameras in stereo configuration is obtained as an extension of the derivation for a single camera. Our approach is to

augment the set of single-camera constraints in (6) by a similar set written for the second camera.

The geometry for this case is shown in figure 4. The initial location of the stereo pair of cameras is as in figure 1. Their next locations are advanced in  $x$  by integer multiples of  $b_m/N$  up to  $b_m$ . The first and last squint angles of one camera to the point P are denoted by  $\alpha_1$  and  $\alpha_N$  in analogy to  $\theta_1$  and  $\theta_N$  of the other.

Equations (6, 7) are replaced here by

$$\begin{aligned} \theta_i &= \tan^{-1} [\Delta y_i^\theta / \Delta x_i] + \phi + n_i^\theta ; & \alpha_i &= \tan^{-1} [\Delta y_i^\alpha / \Delta x_i] + \phi + n_i^\alpha \\ \Delta x_i &= x - b_m(i-1)/(N-1) \\ \Delta y_i^\theta &= y - b_s/2 ; & \Delta y_i^\alpha &= y + b_s/2 ; & i &= 1, 2, \dots, N \end{aligned} \quad (17)$$

Using two identical cameras for stereo justifies the assumption that they have equal noise variances. We also assumed that they have equal (but unknown) misalignments as explained earlier. It is, of course, possible to assume independent misalignments for the two cameras and estimate them both in analogy to the estimation of  $\phi$ . We chose to proceed with the realistic assumption of only a single common misalignment.

Next, we replace (8) here by

$$F_\beta = \begin{bmatrix} G_\theta & 1_N \\ G_\alpha & 1_N \end{bmatrix} \quad (18)$$

which is written in a block-matrix form, where

$$\begin{aligned} G_\theta &= \begin{bmatrix} -\Delta y_1^\theta / r_{\theta 1}^2 & -\Delta y_2^\theta / r_{\theta 2}^2 & \dots & -\Delta y_N^\theta / r_{\theta N}^2 \\ \Delta x_1 / r_{\theta 1}^2 & \Delta x_2 / r_{\theta 2}^2 & \dots & \Delta x_N / r_{\theta N}^2 \end{bmatrix}^T \\ G_\alpha &= \begin{bmatrix} -\Delta y_1^\alpha / r_{\alpha 1}^2 & -\Delta y_2^\alpha / r_{\alpha 2}^2 & \dots & -\Delta y_N^\alpha / r_{\alpha N}^2 \\ \Delta x_1 / r_{\alpha 1}^2 & \Delta x_2 / r_{\alpha 2}^2 & \dots & \Delta x_N / r_{\alpha N}^2 \end{bmatrix}^T \end{aligned} \quad (19)$$

and

$$r_{\theta i}^2 = \Delta x_i^2 + (\Delta y_i^\theta)^2 ; \quad r_{\alpha i}^2 = \Delta x_i^2 + (\Delta y_i^\alpha)^2 ; \quad i = 1, 2, \dots, N \quad (20)$$

Equations (10, 11) similarly transform to

$$\begin{aligned}
S_\beta &= \left\{ \begin{bmatrix} G_\theta & 1_N \\ G_\alpha & 1_N \end{bmatrix}^T (\sigma^2 I_{2N})^{-1} \begin{bmatrix} G_\theta & 1_N \\ G_\alpha & 1_N \end{bmatrix} + \text{diag}(0, 0, \sigma_\phi^{-2}) \right\}^{-1} \\
&= \sigma^2 \begin{bmatrix} V_s^{-1} & H_s \\ H_s^T & (\sigma/\sigma_\phi)^2 + 2N \end{bmatrix}^{-1}
\end{aligned} \tag{21}$$

where  $H_s$  and  $V_s$ , subscripted by s for “stereo”, are defined as

$$H_s \equiv (G_\theta^T + G_\alpha^T) 1_N ; \quad V_s \equiv (G_\theta^T G_\theta + G_\alpha^T G_\alpha)^{-1} \tag{22}$$

The CRLB,  $S_s$ , on the location estimation  $(x, y)$  based on OF from two cameras in stereo configuration is found as in (12)

$$S_s = \sigma^2 \left[ V_s + \frac{V_s H_s H_s^T V_s}{(\sigma/\sigma_\phi)^2 + 2N - H_s^T V_s H_s} \right] \tag{23}$$

When there is no a priori information about the misalignment, (23) becomes

$$S_{s \max} = \lim_{\sigma_\phi \rightarrow \infty} S_s = \sigma^2 \left( V_s + \frac{V_s H_s H_s^T V_s}{2N - H_s^T V_s H_s} \right) \tag{24}$$

and, when the misalignment is known, (23) becomes

$$\lim_{\sigma_\phi \rightarrow 0} S_s = \sigma^2 V_s \tag{25}$$

## 4.2 Interpretation of the Results

### 4.2.1 Least Squares Achieves the CRLB

Returning to (10) and its underlying assumptions, it is easy to see that the CRLB is achievable by a maximum-likelihood (ML) algorithm. Poirot [2] gives a general least-squares (LS) solution to the problem of location/misalignment estimation when the observations are linearized around the correct parameter values. His LS problem is identical to the linearized version of (6), that is, solve

$$\Theta = F_\beta \beta + \epsilon \tag{26}$$

for the parameter vector  $\beta \triangleq (x, y, \phi)$ , where  $\Theta$  is the vector of angle measurements,  $F_\beta$  is given by (8), and  $e$  is the measurement-noise vector having a diagonal covariance matrix  $\Sigma$ . The LS solution [2, 13] is

$$\hat{\beta} = PF_\beta^T \Sigma^{-1} \Theta ; \quad P = (F_\beta^T \Sigma^{-1} F_\beta)^{-1} \quad (27)$$

where  $P$  is the covariance matrix of the estimate error [13], *i.e.*,

$$P \triangleq \text{cov}(\beta - \hat{\beta}) \quad (28)$$

Note from (27) and (10) that, when  $\sigma_\phi \Rightarrow \infty$  (*i.e.*, there is no a priori knowledge about the misalignment magnitude),  $P = S_\beta$ .

#### 4.2.2 Error Ellipses Never Intersect

For a bivariate Gaussian location error, the joint probability density function of the location-error vector,  $r = (\Delta x, \Delta y)$ , is proportional to  $\exp\{-\frac{1}{2}r^T S^{-1} r\}$ . Thus, the equation  $r^T S^{-1} r = c$ , for any positive constant  $c$ , describes an iso-probability ellipse in the plane. We call the ellipse obtained with  $c = 1$  the “error ellipse”.

Let us now examine the two terms inside the brackets of (12) (or (23)) in order to determine their relative effect on the error ellipse. The first term is  $V$  which, being a covariance matrix, is a *positive definite matrix* (PDM). The second term is a rank-1 matrix divided by a scalar. The associated quadratic form of that matrix is  $r^T V H H^T V r = \|H^T V r\|^2$  which is non-negative; thus  $V H H^T V$  is a *positive semi-definite matrix* (PSDM). We will show that the dividing scalar is a small positive number whose effect is to amplify  $V H H^T V$ , *i.e.*, to increase the location errors. Our goal is to show that increasing the stereo baseline increases the value of this number (in (23)) so that the contribution of the second matrix to the errors is mitigated compared to the non-stereo case.

From (11),

$$N - H^T V H = 1_N^T \left( I_N - G(G^T G)^{-1} G^T \right) 1_N. \quad (29)$$

The rank-2  $N \times N$  matrix  $G(G^T G)^{-1} G^T$  is obviously symmetric and idempotent, thus, for any  $N > 2$ , it is a projection matrix (onto the column space of  $G$ ) which must be

a PSDM. In general, if  $M$  is a projection matrix, so is  $I - M$ , thus (29) is recognized as a quadratic form evaluated for the particular vector  $1_N$ . Since  $1_N$  does not lie in the column space of  $G$ , it cannot zero this quadratic form. We thus conclude that  $N - H^T V H$  is a positive scalar which we call “misalignment sensitivity factor” (MSF).

From (15) and (16) it is seen that  $H^T V H$  is  $\propto N$ , so that  $\text{MSF} \propto N$ . Also,  $V \propto 1/N$ , and  $V H H^T V$  is independent of  $N$ . Thus  $S$  (for  $\sigma_\phi \rightarrow \infty$ ) of (12) is  $\propto 1/N$  as expected.

It will be later seen that the value of the MSF of a stereo/OF system is of the order of  $10^{-5}$  when  $b_s = 0$  (*i.e.*, a monocular system), and it increases dramatically (three orders of magnitude) with even a small increase in  $b_s$ . This advantage of stereo becomes apparent when the MSF’s magnitude is compared with that of the additional positive scalar  $(\sigma/\sigma_\phi)^2$  in (12) or in (23) which always increases the denominator — thus mitigates the adverse effect of the matrix  $V H H^T V$  (or  $V_s H_s H_s^T V_s$ ). For typical values of  $\sigma = 0.1^0$  and  $\sigma_\phi = 2^0$ ,  $(\sigma/\sigma_\phi)^2 = 25 \cdot 10^{-4}$  which is 100 times larger than the MSF of a monocular OF but is of the same order of magnitude of the MSF for stereo/OF. Therefore the stereo/OF location variances are almost immune to the value of  $\sigma_\phi$  whereas the monocular OF variances go almost linearly with  $\sigma_\phi^2$ .

It is shown in the appendix that the error ellipse associated with the summation of a PDM  $V$  and a rank-1 matrix  $uu^T$  always encloses and tangential to (touches at two points) the error ellipse associated with  $V$  alone. This result indicates that the ellipses determined by (12) (or (23)) grow with  $\sigma_\phi$  so that each larger ellipse fully encloses the smaller- $\sigma_\phi$  ellipse and all share the *same* two tangent points.

Later we will need the major and minor axes of the error ellipses and their orientation. The necessary results are summarized below [4]. Consider the ellipse  $r^T S^{-1} r = 1$ , associated with a covariance matrix  $S$ , where  $r = (x, y)$  is the location vector in the plane, and denote its components by  $s_{ij}$ ,  $i, j = 1, 2$ . This ellipse has major ( $\sigma_L$ ) and minor ( $\sigma_S$ ) radii equal to the square root of its large and small eigenvalues which are given by

$$\sigma_L^2, \sigma_S^2 = \frac{1}{2} \left[ s_{11} + s_{22} \pm \sqrt{(s_{11} - s_{22})^2 + (2s_{12})^2} \right] \quad (30)$$

where the  $+\sqrt{\cdot}$  corresponds to  $\sigma_L$  and  $-\sqrt{\cdot}$  to  $\sigma_S$ . The major axis is rotated with respect to the  $X$  axis by

$$\gamma = \frac{1}{2} \tan^{-1} \left[ \frac{2s_{12}}{s_{11} - s_{22}} \right]; \quad -\frac{\pi}{4} \leq \gamma \leq \frac{\pi}{4} \quad (31)$$

The directions of the ellipse axes coincide with the direction of the corresponding eigenvectors. In monocular OF with no misalignment, it is easy to find from (12), (16), (30), and (31) that

$$\gamma = \frac{1}{2}(\theta_1 + \theta_N) \quad (32)$$

$$\sigma_L^2 = \frac{2Ly}{N} \frac{\sigma^2}{\theta_d - \sin \theta_d}; \quad \sigma_S^2 = \frac{2Ly}{N} \frac{\sigma^2}{\theta_d + \sin \theta_d} \quad (33)$$

which interestingly orients the major ellipse axis at the exact average of the initial/final squint angles.  $\sigma_L$  of the stereo/OF case is later given by (44).

### 4.3 Evaluating the CRLB for stereo/OF

Approximating all summations involved in  $S_s$  of (23) by integrals as before, yields

$$H_s \approx \frac{N}{b_m} \left[ -(\theta_d + \alpha_d) \quad \ln \frac{\sin \theta_N \sin \alpha_N}{\sin \theta_1 \sin \alpha_1} \right]^T \quad (34)$$

$$V_s^{-1} = \frac{N}{2b_m h_\alpha h_\theta} \begin{bmatrix} h_\alpha(\theta_d - \sin \theta_d \cos \theta_s) & -h_\alpha \sin \theta_s \sin \theta_d \\ +h_\theta(\alpha_d - \sin \alpha_d \cos \alpha_s) & -h_\theta \sin \alpha_s \sin \alpha_d \\ -h_\alpha \sin \theta_s \sin \theta_d & h_\alpha(\theta_d + \sin \theta_d \cos \theta_s) \\ -h_\theta \sin \alpha_s \sin \alpha_d & +h_\theta(\alpha_d + \sin \alpha_d \cos \alpha_s) \end{bmatrix} \quad (35)$$

where

$$h_\theta \triangleq y - b_s/2; \quad h_\alpha \triangleq y + b_s/2 \quad (36)$$

and

$$\theta_d \triangleq \theta_N - \theta_1; \quad \theta_s \triangleq \theta_N + \theta_1; \quad \alpha_d \triangleq \alpha_N - \alpha_1; \quad \alpha_s \triangleq \alpha_N + \alpha_1 \quad (37)$$

with  $\theta_1, \theta_N, \alpha_1, \alpha_N$  the initial and final squint angles for the two cameras as defined in figure 4.  $V_s$  is obtained by inverting (35); the determinant of this inversion is

$$\Delta = h_\alpha^2(\theta_d^2 - \sin^2 \theta_d) + h_\theta^2(\alpha_d^2 - \sin^2 \alpha_d) + 2h_\theta h_\alpha [\theta_d \alpha_d - \sin \theta_d \sin \alpha_d \cos(\alpha_s - \theta_s)] \quad (38)$$

The above completes the evaluation of all terms in (23). The resulting  $2 \times 2$  matrix,  $S_s$ , describes the estimation errors in the  $(X, Y)$  plane.

#### 4.4 Small-angle approximations to the CRLB for stereo/OF

The above CRLB expressions for stereo/OF are too cumbersome to be readily interpreted. For the zero-misalignment case we will derive approximate expressions which allow some interesting insight.

Let us assume a narrow field of view of, say,  $\pm 15^\circ$ ,  $b_m \ll x$ , and  $b_s \ll y$  which allows the approximations

$$\sin x \approx x - x^3/6 : \cos x \approx 1 - x^2/2 : h_\alpha \approx h_\theta \approx y : \theta_s \approx 2\theta_1 : \alpha_s \approx 2\alpha_1 \quad (39)$$

Starting with  $V_s$  of (35), the terms appearing in its determinant (38) are

$$\begin{aligned} \theta_d^2 - \sin^2 \theta_d &\approx \frac{\theta_d^4}{3} ; \alpha_d^2 - \sin^2 \alpha_d \approx \frac{\alpha_d^4}{3} ; \sin \theta_d \sin \alpha_d \approx \theta_d \alpha_d - \frac{\theta_d \alpha_d^3}{6} - \frac{\theta_d^3 \alpha_d}{6} \\ \theta_1 &\approx \theta_N ; \alpha_1 \approx \alpha_N ; \theta_s \approx 2\theta_1 \approx 2\frac{y - b_s/2}{x} ; \alpha_s \approx 2\alpha_1 \approx 2\frac{y + b_s/2}{x} ; \alpha_s - \theta_s = 2b_s/x \end{aligned} \quad (40)$$

so that

$$\Delta \approx 4y^2 \theta_d^2 \left( \frac{\theta_d^2}{3} + \frac{b_s^2}{x^2} \right) \quad (41)$$

Note that  $\Delta$  and the other approximated expressions can alternatively be written in terms of difference and sum angles based on  $\alpha$  or on  $\theta$  since  $\alpha_d \approx \theta_d$  and  $\alpha_s \approx \theta_s$ . Approximating the difference angle  $\theta_d$  by  $b_m \theta_1/x$ ,

$$\Delta \approx \frac{4y^2 b_m^2 \theta_1^2}{x^4} \left( \frac{b_m^2 \theta_1^2}{3} + b_s^2 \right) \quad (42)$$

The approximate expressions for the matrix elements of  $V_s$  can be similarly found so that

$$V_s \approx \frac{2yx^3}{N(b_m^2 \theta_1^2/3 + b_s^2)} \begin{bmatrix} 1/\theta_1 & 1 \\ 1 & \theta_1 \end{bmatrix} \quad (43)$$

The covariance matrix of (43) is inevitably singular because of the first-order approximations used in its derivation. Singularity only means that the error ellipse degenerates into its major axis (a line), *i.e.*, its minor axis equals zero. Higher-order approximations are needed to find the minor axis. From (30), we have

$$\sigma_L \approx \frac{\sqrt{2}x^2}{\sqrt{N}f\sqrt{b_m^2\theta_1^2/3 + b_s^2}}\sigma_u \quad (44)$$

where we have used  $\theta_1 \approx y/x \approx u_1/f$ ;  $\sigma = \sigma_u/f$ .

It is interesting to compare the above results with those of section 2. Setting  $b_m = 0$  in (44) degenerates it to reflect only *stationary* stereo errors, that is,

$$\sigma_L \approx \frac{\sqrt{2}x^2}{\sqrt{N}fb_s}\sigma_u \quad (45)$$

This result is expected since it only differs from (3) by a factor of  $\sqrt{N}$ . This is because all  $N$  stereo measurements are collocated and independent; thus the CRLB is met by a simple averaging algorithm.

Setting  $b_s = 0$  in (44) degenerates it to reflect monocular-OF errors because it forces the stereo camera pair to be collocated. To obtain results for a single, rather than for two collocated traveling cameras, the variance result has to be doubled, *i.e.*,

$$\sigma_L \approx \frac{\sqrt{12}x^2}{\sqrt{N}u_1b_m}\sigma_u \quad (46)$$

which is  $\sqrt{6/N}$  times the  $\sigma_x$  in (4). The factor of  $1/N$  accounts for the  $N$  independent measurements. The factor of 6 reflects averaging on the changing geometry during the OF observation time.

## 5 Simulation Results

In this section we present simulation results that exemplify the predicted theoretical behavior. Unless stated otherwise, all cases assume ranging an object at  $x = 150$  m, observation time:  $T = 1.5$  s, sampling time:  $\Delta T = 0.05$  s, noise rms:  $\sigma = 0.1^\circ$ , and

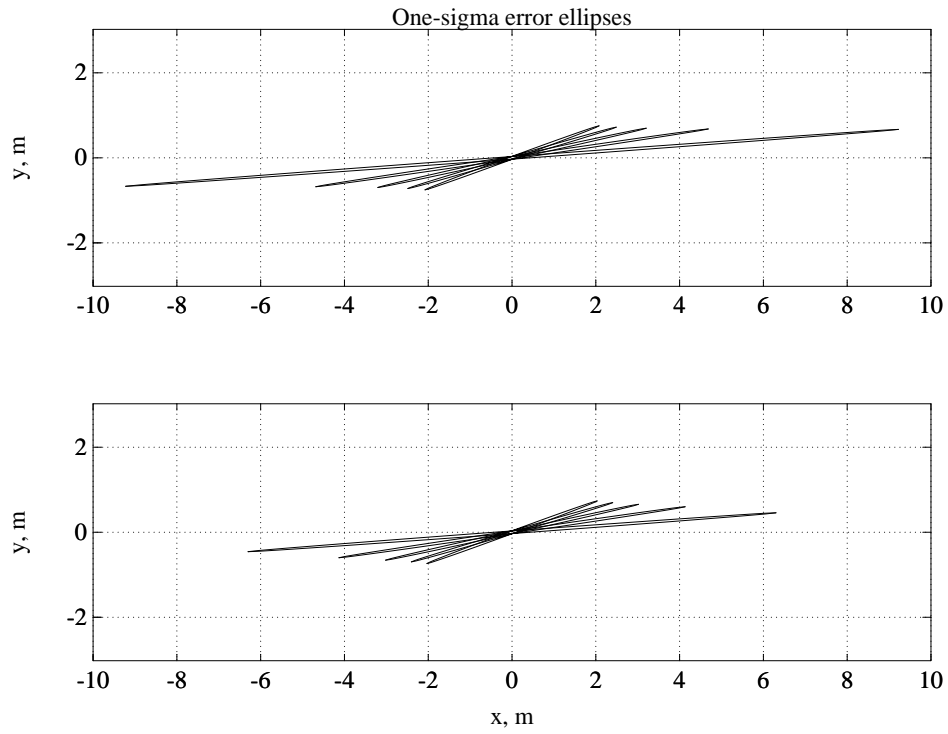


Figure 5: Error ellipses:  $b_s = 0$  (t),  $= 1$  m (b),  $V = 15$  m/s, no misalignment.

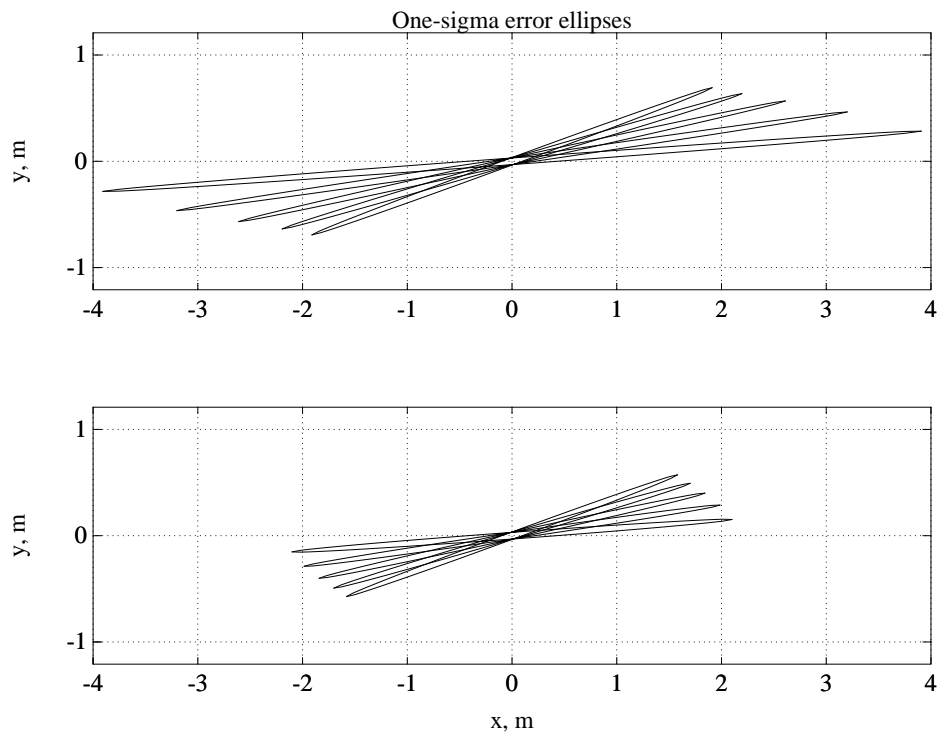


Figure 6: Error ellipses:  $b_s = 2$  (t)  $= 4$  m (b),  $V = 15$  m/s, no misalignment.

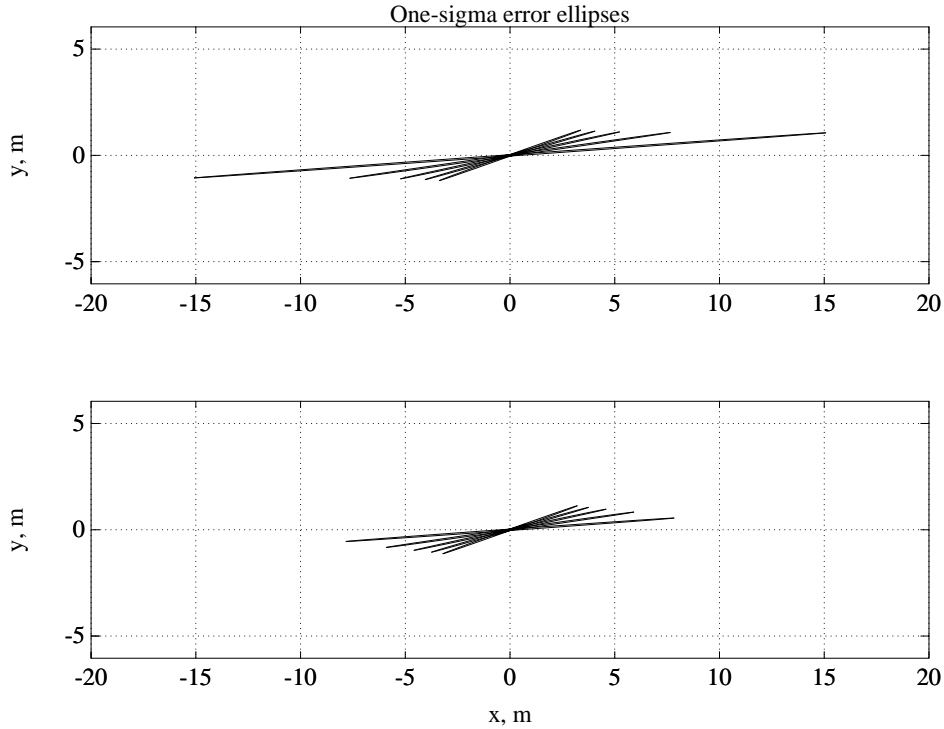


Figure 7: Case similar to figure 5 but with  $V = 10$  m/s

lateral object distance:  $y = 10, 20, 30, 40, 50$  m. The noise rms was chosen to represent half a pixel for a camera that employs a  $512 \times 512$  detector and covers a field of view of  $102^\circ$ . The other parameters are specified for each case.

Let us start with zero-misalignment cases. Figure 5 shows such a case for a vehicle speed of  $V = 15$  m/s and two values for the stereo baseline:  $b_s = 0, 1$  m. The ellipses can be thought to be centered on point P of figure 4. All have a major axis in the line-of-sight direction which is much larger than their minor axis. The ellipses are shown in their correct angular position. Thus the longest ellipse belongs to  $y = 10$  m and its major axis is at  $0.0725$  rad from the flight path which is the average angle between  $10/150$  and  $10/127.5$  rad ( $VT = 22.5$  m). The shortest ellipse belongs to  $y = 50$  m. Clearly, the depth accuracy improves as  $y$  (or  $\theta$ ) increases. The corresponding ellipses for  $b_s = 1$  are smaller, and also the ratio between the  $y = 50$  m — and  $y = 10$  m — ellipses is smaller as compared to the  $b_s = 0$  m case. The non-zero stereo baseline is, of course, the reason for the improved accuracy which is relatively more pronounced at small squint angles as

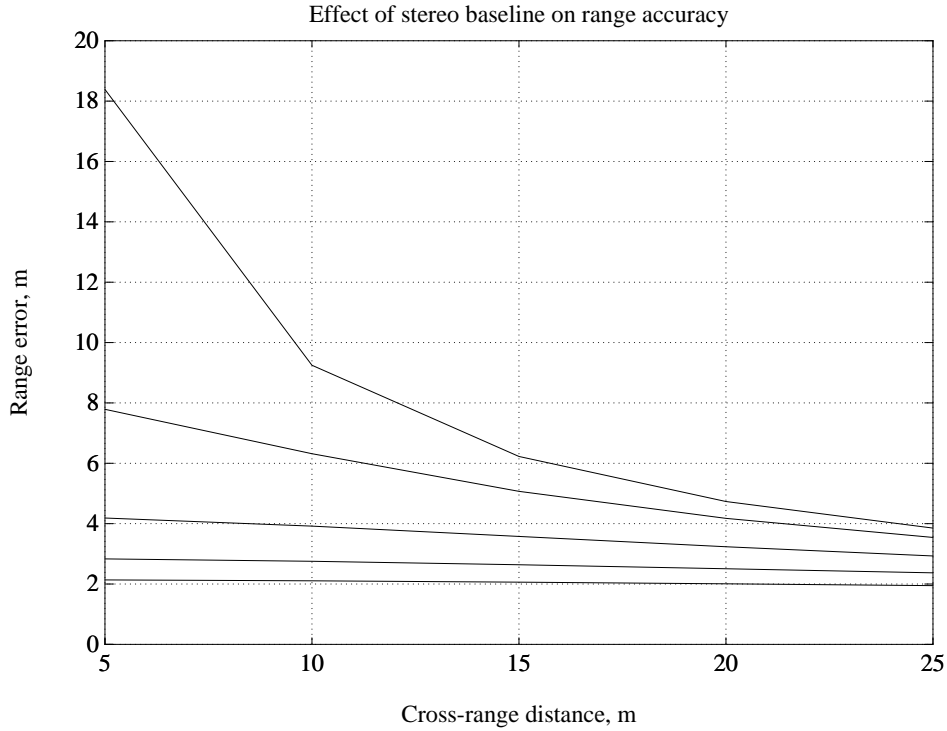


Figure 8: Depth errors for  $b_s = 0, 1, 2, 3, 4$  m,  $V = 15$  m/s, no misalignment seen in (44).

Figure 6 is similar to figure 5 except that the stereo baseline has values of  $b_s = 2, 4$  m. Here the ellipses justify their name better because the major axis has decreased considerably with increasing  $b_s$ . Figure 7 is similar to figure 5 but for  $V = 10$  m/s instead of  $V = 15$  m/s which makes the OF baseline,  $b_m$ , 1.5 times shorter. This causes the case of  $b_s = 0$  (top) to show ellipses which are longer by 50%. On the other hand, in the case of  $b_s = 1$  m the accuracies are only degraded by about 15% for small squint angles.

The effect of stereo baseline, vehicle speed, and cross-depth (squint angle) are summarized in figures 8, for  $V = 15$  m/s, and figure 9, for  $V = 10$  m/s. It is seen that increasing  $b_s$  has the largest effect when the squint angles are small, and that, for a large  $b_s$ , the depth errors become insensitive to the vehicle speed.

Now we investigate the effect of stereo baseline on the MSF,  $2N - H_s^T V_s H_s$ , in (24). The MSF is a very small positive number whose inverse directly amplifies the matrix

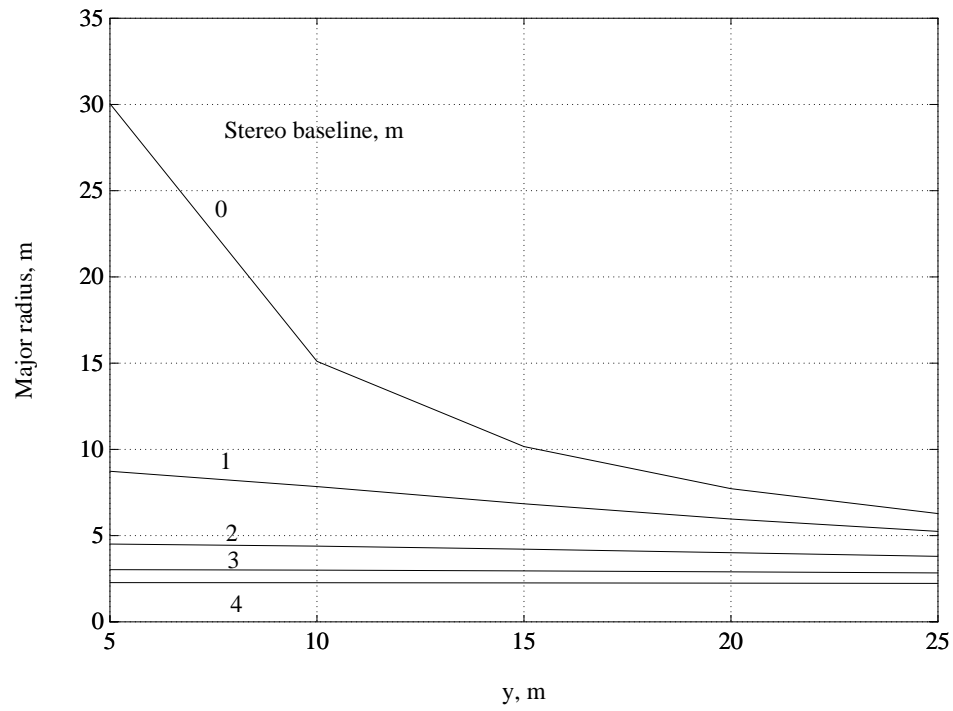


Figure 9: Case similar to figure 8 but with  $V = 10$  m/s

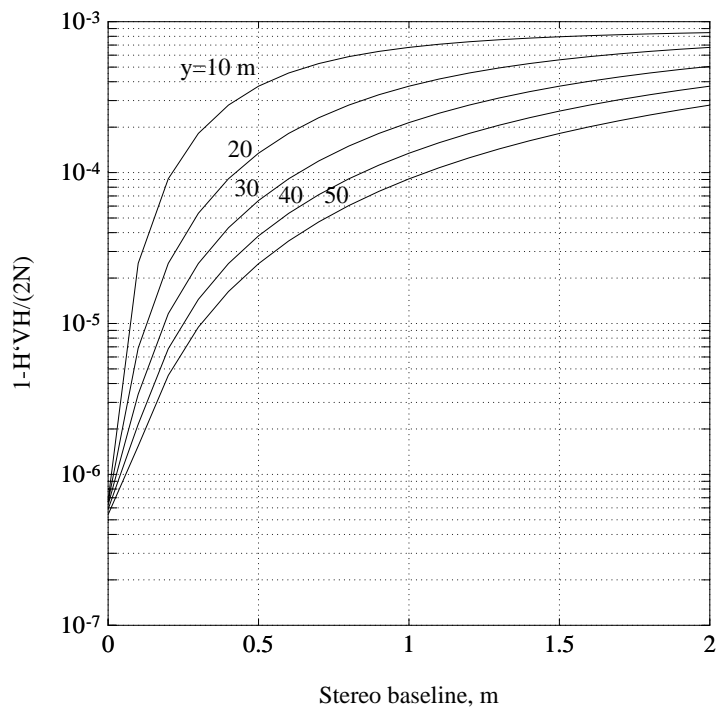


Figure 10: Misalignment sensitivity factor for  $V = 10$  m/s,  $y = 10$  m to 50 m

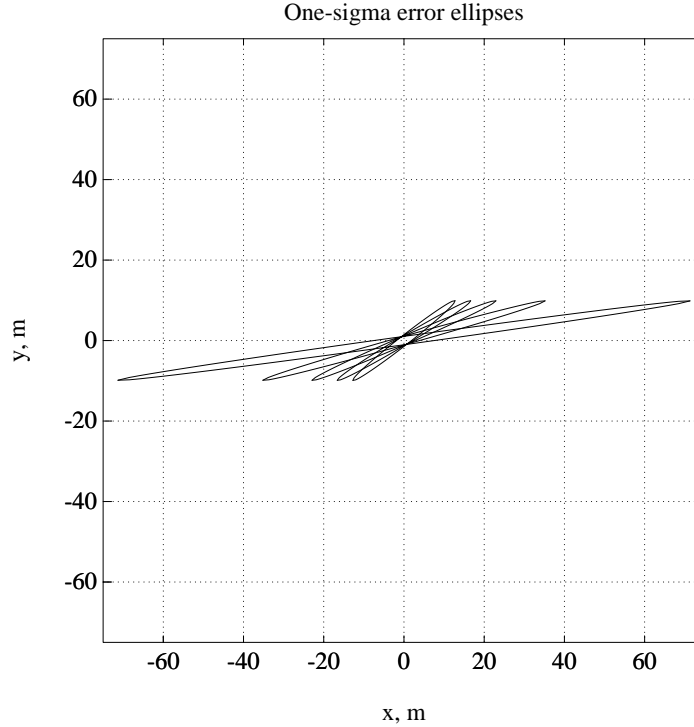


Figure 11: Error ellipses for  $V = 10$  m/s,  $y=10$  to  $50$  m,  $\sigma_\phi = 2^\circ$ ,  $\sigma = 0.1^\circ$ ,  $b_s = 0$  m

$V_s H_s H_s^T V_s$  when the misalignment is completely unknown; it is given (normalized by  $2N$ ) in figure 10 for  $V = 10$  m/s and  $y = 10$  to  $50$  m. It is seen that the MSF increases dramatically with the stereo baseline — up to 3 orders of magnitude; this establishes one of our most important conclusions. The effect of this factor will now be translated directly to the error ellipses.

In the sequel we differentiate between the major ellipse axis and the depth (or line-of-sight) direction because they turn out to be different in the case of an unknown misalignment. Two sets of error ellipses are shown in figures 11 (for  $b_s = 0$ ) and in figures 12 (for  $b_s = 1$  m). It is seen that even a small stereo baseline of 1 m decreases the major ellipse axis for small squint angles by a factor of 10. Interestingly, in this case the major axes for stereo become constant — irrespective of the squint angle. This “equalization” effect only shows up in the unknown-misalignment case as compared with the similar case (but with no misalignment) shown in figure 7. This comparison also shows that an unknown misalignment ( $\sigma_\phi = 2^\circ$ ) increases the major axes by a factor of

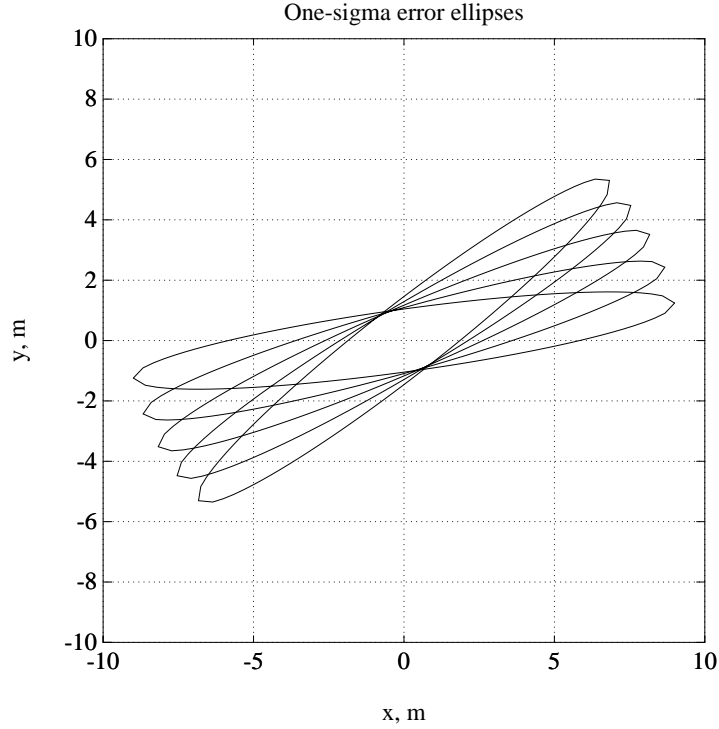


Figure 12: Similar to figure 11 but with  $b_s = 1$  m

$\approx 5$  compared to a zero-misalignment monocular OF as opposed to only a factor of  $\approx 1.2$  (for small squint angles) up to  $\approx 2.2$  (for large squint angles) for stereo with  $b_s = 1$  m.

Figure 13 summarizes the effect of stereo baseline on the major axes in the presence of unknown misalignment. It is seen that the major axis becomes virtually constant with respect to the cross-depth for  $b_s > 0.5$  m, and that this constant is inversely proportional to  $b_s$ .

Figures 14 and 15 show the effect of stereo on the error ellipses. In general, the zero-misalignment ellipses are narrow so that their apexes are very close to the points of tangency with the misalignment ellipses. Since the major axes of the zero-misalignment ellipses coincide with the depth direction, we conclude that the misalignment ellipses show almost the same *depth* accuracy although their major axis is much larger. We, thus, compare cases by their major axis.

Figure 14 shows the error ellipses resulting from misalignment errors of  $\sigma_\phi =$

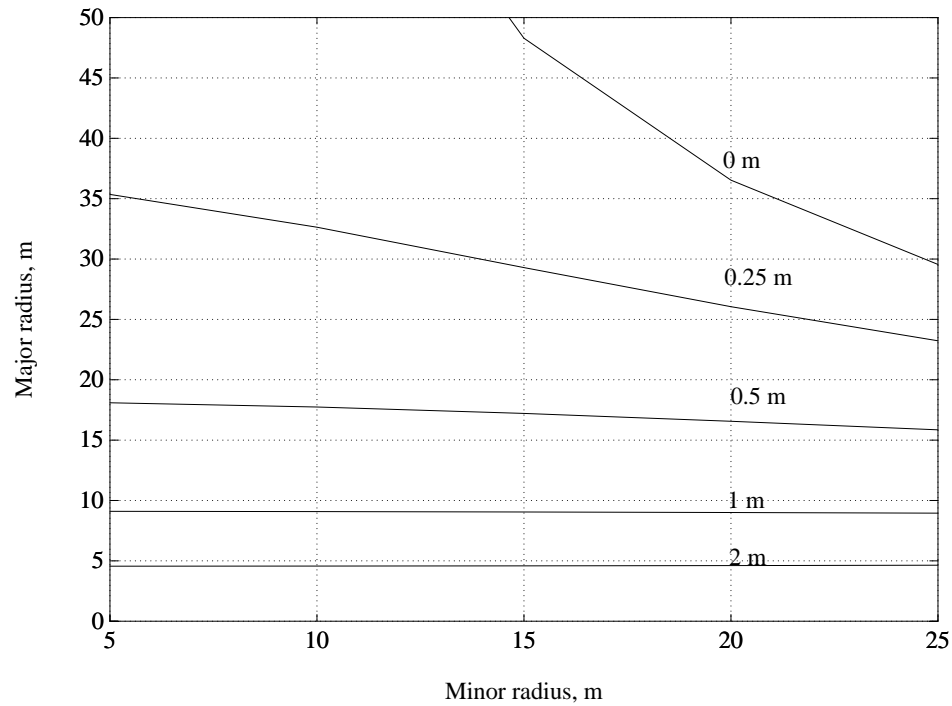


Figure 13: Effect of stereo baseline,  $V = 10$  m/s,  $\sigma_\phi = 2^\circ$ ,  $\sigma = 0.1^\circ$ ,  $b_s = 0$  to 2 m

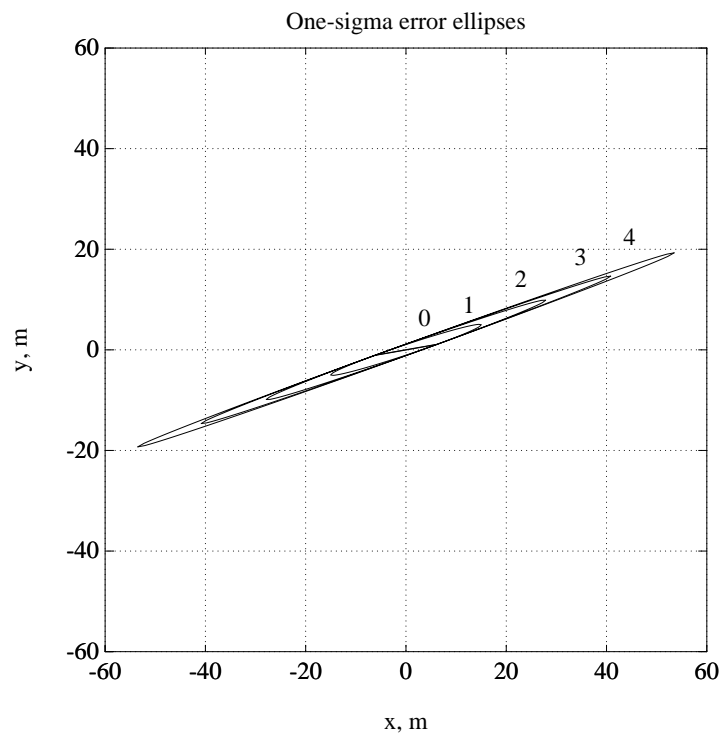


Figure 14: Effect of misalignment,  $b_s = 0$  m,  $V = 10$  m/s,  $y = 25$  m  $\sigma_\phi = 0$  to  $4^\circ$ ,  $\sigma = 0.1^\circ$

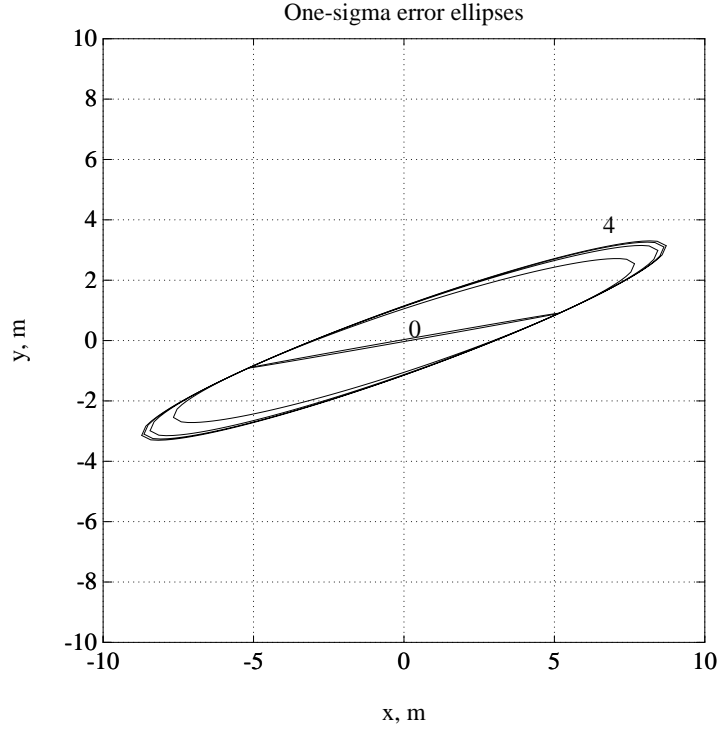


Figure 15: Same as figure 14 except that  $b_s = 1$  m

0, 1, 2, 3, 4<sup>0</sup> for the case of  $y = 25$  m,  $V = 10$  m/s and  $b_s = 0$ . It is seen that the major axes grow, close to linearly with  $\sigma_\phi$ , from 5 m to 60 m. This happens because the MSF is negligible compared to  $(\sigma/\sigma_\phi)^2$  in (23). Figure 15 shows the same case as figure 14 except that  $b_s = 1$  m. Here, since the MSF is  $\approx 3$  orders of magnitude larger, ellipses corresponding to  $\sigma_\phi \geq 2^0$  are already close to the asymptotic ellipse of (24) which has a major axis only twice as large as in the zero-misalignment case.

## Appendix

In this appendix we show that the error ellipse

$$r^T V^{-1} r = 1 \quad (47)$$

in the location-error plane  $r = (\Delta x, \Delta y)$  is enclosed by and tangential to the error ellipse

$$R^T (V + uu^T)^{-1} R = 1 \quad (48)$$

which is written for the generally-different vector  $R$ .

Consider a vector  $r$  that belongs to the (47) ellipse. We will first show that the *same* vector has to be elongated by a factor  $a > 1$  in order to reach the ellipse of (48) — meaning that the latter ellipse is farther away from the origin at all its points. To do that, (48) is rewritten, using the matrix inversion formula [12], as

$$R^T \left( V^{-1} - \frac{V^{-1}uu^TV^{-1}}{1 + u^TV^{-1}u} \right) R = 1 \quad (49)$$

Plugging  $R = ar$  into (49) and dividing both sides of the equation by  $a^2$ ,

$$r^TV^{-1}r - r^T \frac{V^{-1}uu^TV^{-1}}{1 + u^TV^{-1}u} r = \frac{1}{a^2} \quad (50)$$

Now, using (47),

$$\frac{a^2 - 1}{a^2} = r^T \frac{V^{-1}uu^TV^{-1}}{1 + u^TV^{-1}u} r \quad (51)$$

For a PDM  $V$ ,  $u^TV^{-1}u$  is a positive scalar. Also,  $r^TV^{-1}uu^TV^{-1}r = \|u^TV^{-1}r\|^2 > 0$ , thus the right-hand side of (51) is a positive scalar which can only be satisfied on the left-hand side by an  $a > 1$ .

Now we want to prove that both ellipses are tangential. Returning to (49), it is seen that, for a vector  $R^\perp$  orthogonal to  $V^{-1}u$ , the inner product  $u^TV^{-1}R^\perp = 0$ ; this will zero out the second matrix inside the parenthesis. For that vector only, (49) takes the form of (47) — meaning that this vector intersects the ellipses of (47), and (48) at their two tangential points.

## 6 Summary and Conclusions

In this paper we developed the CRLB for the location errors of a combined stereo/optical-flow system in the presence of misalignment between the stereo camera pair and the INS. It has been shown that even a very small stereo baseline decreases the errors by a large factor. The error analysis in this work can serve to guide the design and choice of parameters for a passive obstacle-avoidance system.

## References

- [1] Stansfield, R., "Statistical Theory of DF Fixing", *Journal IEEE*, Vol. 94 Part 3A, n 15, 1947, pp. 762-770.
- [2] Poirot, J.L., and G.V. McWilliams, "Application of Linear Statistical Models to Radar Location Techniques", *IEEE Transactions on Aerospace and Electronic Systems*, Vol. AES-10, No. 6, Nov. 1974, pp. 830-834.
- [3] Spingarn, K., "Passive Position Location Estimation Using the Extended Kalman Filter", *IEEE Transactions on Aerospace and Electronic Systems*, Vol. AES-23, No. 4, July 1987, pp. 558-567.
- [4] Torrieri, D.J., "Statistical Theory of Passive Location Systems", *IEEE Transactions on Aerospace and Electronic Systems*, Vol. AES-20, No. 2, March 1984, pp. 183-198.
- [5] Wegner, L.H., "On the Accuracy Analysis of Airborne Techniques for Passively Locating Electromagnetic Emitters," *Report R-722-PR, Rand Corp.*, NTIS ASTIA D.C. AD 729 767, 1971.
- [6] Gavish, M., and E. Fogel, "Effect of Bias on Bearing-Only Target Location", *IEEE Transactions on Aerospace and Electronic Systems*, Vol. 26, No. 1, Jan 1990, pp. 22-25.
- [7] Matthies, L., R. Szeliski, T. Kanade, "Kalman Filter-based Algorithms for Estimating Depth from Image Sequences", *CMU-CS-87-185*, Dec. 1987.
- [8] Sridhar, B., A.V. Phatak, "Simulation and Analysis of Image-based Navigation System for Rotorcraft Low-altitude Flight", *AHS National Specialists' Meeting Automation Application of Rotorcraft*, Atlanta, GA, April 4-6 1988.
- [9] Menon, P.K.A., and B. Sridhar, "Passive Navigation Using Image Irradiance Tracking", *AIAA Guidance, Navigation and Control Conference, Boston, MA*, Paper No. 89-3500, Aug. 14-16 1989, pp 639-646.

- [10] Barniv Y., "Application of Velocity filtering to Optical-Flow Passive Ranging", *IEEE Transactions on Aerospace and Electronic Systems*, (to be published around July 1991).
- [11] Sridhar, B., and R. Suorsa, "Integration of Motion and Stereo Sensors in Passive Ranging Systems," *American Control Conference*, San Diego, CA, May 1990.
- [12] Kailath, T., *Linear Systems*, Englewood Cliffs, NJ: Prentice-Hall, 1980, pp. 655-656.
- [13] Nahi, N.E., *Estimation Theory and Applications*, Wiley, NY, 1969, 656.